Received: 14 December 2022 | Revised: 28 February 2023 | Accepted: 1 March 2023

DOI: 10.1002/pro.4616

FOR THE RECORD

Monomer and dimer structures of cytochrome bo_3 ubiquinol oxidase from *Escherichia coli*

Yirui Guo[1,2] | **Elina Karimullina**[3,4,5] | **Tabitha Emde**[1,4,5] | **Zbyszek Otwinowski**[1,4,5,6] | **Dominika Borek**[1,4,5,6] | **Alexei Savchenko**[3,4,5,7]

[1]Department of Biophysics, The University of Texas Southwestern Medical Center, Dallas, Texas, USA

[2]Ligo Analytics, Dallas, Texas, USA

[3]Department of Microbiology, Immunology and Infectious Diseases, University of Calgary, Calgary, Alberta, Canada

[4]Center for Structural Genomics of Infectious Diseases (CSGID), Chicago, Illinois, USA

[5]Centers for Research on Structural Biology of Infectious Diseases (CSBID), Chicago, Illinois, USA

[6]Department of Biochemistry, The University of Texas Southwestern Medical Center, Dallas, Texas, USA

[7]BioZone, Department of Chemical Engineering and Applied Chemistry, University of Toronto, Toronto, Ontario, Canada

Correspondence
Dominika Borek and Alexei Savchenko, Center for Structural Genomics of Infectious Diseases (CSGID), Chicago, IL, USA.
Email: dominika.borek@utsouthwestern.edu and alexei.savchenko@ucalgary.ca

Funding information
Department of Energy, Office of Science, Grant/Award Numbers: DE-SC0019600, DE-SC0021600; Cancer Prevention and Research Institute of Texas, Grant/Award Numbers: RP170644, RP220582; National Institute of Allergy and Infectious Diseases, Grant/Award Numbers: 75N93022C00035, HHSN272201700060C; National Institute of General Medical Sciences, Grant/Award Number: R35GM145365

Review Editor: Jeanine Amacher

Abstract

The *Escherichia coli* cytochrome bo_3 ubiquinol oxidase is a four-subunit heme-copper oxidase that serves as a proton pump in the *E. coli* aerobic respiratory chain. Despite many mechanistic studies, it is unclear whether this ubiquinol oxidase functions as a monomer, or as a dimer in a manner similar to its eukaryotic counterparts—the mitochondrial electron transport complexes. In this study, we determined the monomeric and dimeric structures of the *E. coli* cytochrome bo_3 ubiquinol oxidase reconstituted in amphipol by cryogenic electron microscopy single particle reconstruction (cryo-EM SPR) to a resolution of 3.15 and 3.46 Å, respectively. We have discovered that the protein can form a dimer with C2 symmetry, with the dimerization interface maintained by interactions between the subunit II of one monomer and the subunit IV of the other monomer. Moreover, the dimerization does not induce significant structural changes in the monomers, except the movement of a loop in subunit IV (residues 67–74).

KEYWORDS
cryo-EM, cryogenic electron microscopy, dimer, *E. coli* cytochrome bo_3 ubiquinol oxidase

1 | INTRODUCTION

The *Escherichia coli* cytochrome bo_3 ubiquinol oxidase is a heme-copper oxidase that reduces molecular oxygen to water while pumping protons across the membrane (Figure 1) (Abramson et al., 2000; Li et al., 2021; Su et al., 2021). The protein has four subunits and catalyzes the four-electron reduction of O_2 to H_2O. The natural substrate of this enzyme is ubquinol-8. The redox center of the oxidase is located in subunit I, as shown in Figure 1b, with all the cofactors represented in their exact positions in the solved structure. During

This is an open access article under the terms of the Creative Commons Attribution-NonCommercial License, which permits use, distribution and reproduction in any medium, provided the original work is properly cited and is not used for commercial purposes.
© 2023 The Authors. *Protein Science* published by Wiley Periodicals LLC on behalf of The Protein Society.

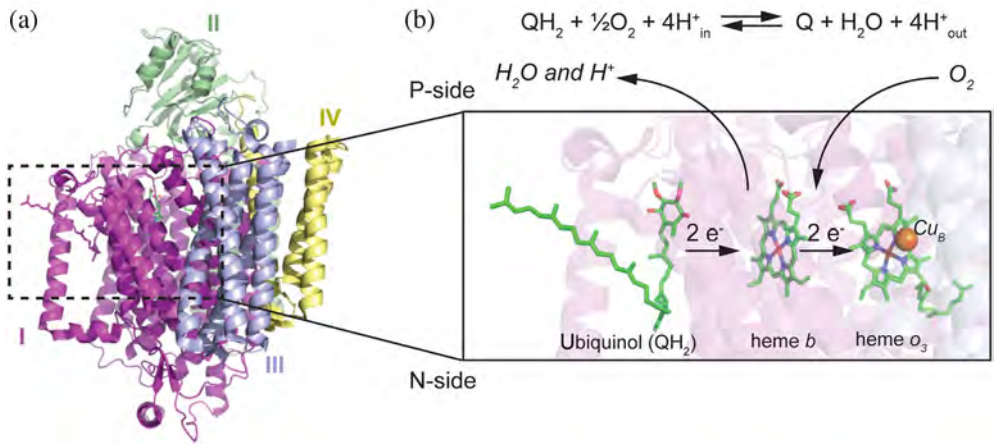

FIGURE 1 Structural and functional overview of the *E. coli* ubiquinol oxidase. *Source*: Adapted from PDB 1FFT and 6WTI. (a) Structure of the *E. coli* ubiquinol oxidase with the four subunits (I, II, III, and IV) shown in different colors. Black dashed box indicates the redox center of the protein. (b) Schematic representation of electron/proton transfer at the redox center. Briefly, all redox centers (ubiquinol, heme *b*, heme o_3, and a copper ion) are bound to subunit I, the largest subunit of the oxidase. Oxidation of one ubiquinol releases two protons on the positive side (P-side) of the membrane ($2H^+$ chemistry). This reaction also creates a proton motive force which pumps two additional protons across the membrane ($2H^+$ translocation).

catalysis, electrons move in the direction from ubiquinol to heme *b* to heme o_3/Cu ion (Cu_B). Protons produced in the reaction are released to the positive side (P-side) of the membrane and are subsequently converted to energy through the aerobic respiratory chain (Puustinen et al., 1989).

The *E. coli* cytochrome bo_3 ubiquinol oxidase is often compared to its eukaryotic counterparts, the mitochondrial electron transport complexes such as the mitochondrial cytochrome bc_1 and cytochrome *c* oxidase. Both mitochondrial electron transport complexes crystalize as dimers and the dimer is believed to be important for proton translocation (Tsukihara et al., 1996; Yu et al., 1998; Zhang et al., 1998; Sone and Kosako, 1986). The dimerization of the mitochondrial electron transport complexes is sensitive to detergent solubilization. For example, cytochrome *c* can switch from a mixture of monomers and dimers to monomers only as detergent concentration increases (Robinson and Talbert, 1986).

However, the quaternary structure of the *E. coli* cytochrome bo_3 ubiquinol oxidase is less clear. Up-to-date, all published structures of this ubiquinol oxidase are monomeric, with only a few structural differences between each other (Abramson et al., 2000; Li et al., 2021; Su et al., 2021). Firstly, the structure solved by X-ray crystallography is missing density in subunit I (residues 552–656) compared to the structures solved by Cryo-EM (Abramson et al., 2000). Secondly, the crystal structure lacks ubiquinone co-factor due to the detergent used in the crystallization conditions, while both cryo-EM structures show one ubiquinone molecule bound to subunit I (Puustinen et al., 1996). Several biochemical and biophysical characterizations of the oligomeric state of the enzyme resulted in contradictory results. Musatov et al. (1999) measured the oligomeric state by sedimentation equilibrium and sedimentation velocity experiments and reported that the detergent-solubilized *E. coli* cytochrome bo_3 ubiquinol oxidase is either monomeric or is highly aggregated; while another study by Stenberg et al. (2007) reported the presence of ubiquinol oxidase dimer detected by blue native polyacrylamide gel electrophoresis (BN-PAGE). The dimer measured by BN-PAGE is roughly 50-fold less abundant than the monomer and is likely sensitive to detergent solubilization.

With the recent developments in cryo-EM SPR which facilitate heterogeneous sample processing and AI-based particle picking (Skalidis et al., 2022; Si et al., 2022), we were able to isolate and computationally enrich the rare dimeric ubiquinol oxidase particles from the sample that was dominated by the highly abundant monomeric particles and solved both structures, including the first dimeric structure of this protein.

2 | METHODS

2.1 | Protein expression and purification

The *E. coli* cytochrome bo_3 ubiquinol oxidase in this study is a byproduct (impurity) of the expression and purification of a recombinant *E. coli* ZapG/RodZ complex. The N-terminally 6His-TEVcleavage site-tagged *E. coli* ZapG (MCS1) and untagged RodZ (MCS2) genes in the petDUET1 vector were transformed into C43 (DE3) competent cells. Transformants were used to inoculate 3 L of LB media with ampicillin (100 μg/mL) at 37°C

until OD600 reached 0.6. The culture was then incubated on ice for 1 hr, induced with 1 mM isopropyl-β-D-thiogalactopyranoside (IPTG) and grown overnight at 20°C. Cells were harvested by centrifugation, resuspended with 1× PBS pH 7.4 and lysed using serial freezing and thawing cycles in the presence of phenylmethylsulfonyl fluoride (PMSF, 0.5 mM), DNase1 (20 μg/mL), lysozyme (1 mg/mL), and TCEP (0.5 mM). All further purification steps were conducted at 4°C. Cells were processed in a cell disruptor (Avastin) at 15,000 psi, three passes. Cell debris was spun down at 13,500×*g* for 20 min. The supernatant was further ultracentrifuged for 1 hr 40 min at 40,000 rpm. The pellet (crude membrane preparation) was washed with 1× PBS containing 0.5 mM TCEP and ultracentrifuged again at 40,000 rpm for 1 hr 30 min. Isolated membrane pellet was frozen and kept at −80°C until the next step. The crude membrane preparation was resuspended in the extraction buffer (50 mM Na Phosphate pH 7.6, 300 mM NaCl, 20% [v/v] glycerol, 0.5 mM TCEP, 1% DDM) and incubated for 2 hr. After ultracentrifugation (40 min, 40,000 rpm), the supernatant was incubated overnight with 3 mL Ni-NTA beads (Qiagen) preequilibrated with the extraction buffer. The next day, the beads were washed with 30 mL of wash 1 (50 mM Na phosphate pH 7.6, 500 mM NaCl, 15% [v/v] glycerol, 0.5 mM TCEP, 40 mM imidazole, 0.1% [w/v] DDM) and wash 2 (50 mM Na Phosphate pH 7.6, 300 mM NaCl, 10% [v/v] glycerol, 0.5 mM TCEP, 50 mM imidazole, 0.05% [w/v] DDM) buffers and then eluted with 15 mL of the elution buffer (50 mM Na phosphate pH 7.6, 300 mM NaCl, 5% [v/v] glycerol, 0.5 mM TCEP, 0.05% [w/v] DDM, 300 mM imidazole). The eluate was dialyzed overnight with TEV protease (purified in-house) in dialysis buffer (50 mM Tris pH 8.0, 300 mM NaCl, 5% [v/v] glycerol, 0.5 mM TCEP, 0.05% [w/v] DDM). The next day, an immobilized metal affinity chromatography (IMAC) column packed with Ni-NTA beads (Qiagen) was used for the second time where the flow-through fraction was passed five times through the column so that all His-tag labeled molecules were retained. Amphipol A8-35 (Anatrace) was added to the flow-through in a 1:3 (w/w) protein: amphipol ratio and incubated with gentle rotation. After 4 hr of rotation, Bio-Beads (Biorad) (15 mg of beads per 1 mL of protein solution) were added and incubated overnight. The next day, the sample with proteins stabilized in amphipol was poured over an empty column to remove the Bio-Beads and concentrated using a 100 kDa cut-off centrifugal concentration device (Amicon). The concentrated sample was loaded on a Superdex 200 Increase 10/300 column equilibrated with detergent free buffer (50 mM Tris pH 8.0, 150 mM NaCl, 0.5 mM TCEP) (Figure S1). The peaks' fractions were collected, concentrated, aliquoted to 15 μL portions, and flash frozen in liquid nitrogen for preparation of grids for cryo-EM single particle reconstruction. Aliquots were kept frozen at −80°C until grids were prepared.

2.2 | Cryo-EM grid preparation and data collection

The purified samples were applied to Quantifoil R 1.2/1.3300 Mesh Gold grids. The grids were glow discharged for 90 s at 30 mA with a PELCO easiGlow™ Glow Discharge Cleaning System to obtain a hydrophilic surface. The glow-discharged grids were used to prepare vitrified samples with the Thermo Scientific Vitrobot Mark IV System. We applied 3 μL of purified protein to the glow-discharged surface of the grid at 4°C at 100% of humidity and blotted the solution for 5.0–5.5 s, with blot force of either 18 or 19.

The data were acquired with a 300 kV Titan Krios G2 microscope (Thermo Fisher) equipped with a K3 Summit direct electron camera (Gatan) run in super-resolution mode at a nominal magnification of 105,000×, with a physical pixel of 0.834 Å. A phase plate was not used and the objective aperture was not inserted. SerialEM was used for automated data collection in beam-image shift mode with nine images collected per stage movement, with a defocus range from −1.0 to −3.0 μm and beam-image shift compensation (Mastronarde, 2005). The slit width of the GIF Quantum Energy Filter was set to 25 eV. Movies were dose-fractionated into 100 frames with a total dose of ~80 $e^{-}/Å^{2}$. Two batches of data were collected. The first batch consisted of 2398 movies, and the second batch consisted of 4509 movies.

2.3 | Cryo-EM image processing and model building

All movies were imported into CryoSPARC followed by patch motion correction using binning of 2 and patch CTF correction (Punjani et al., 2017). Particles were first picked using blob picker on 500 micrographs collected in the first batch to generate initial 2D templates. Templates were created from selected 2D classes and template picking on all micrographs from the first batch was conducted, resulting in a total of 1,498,114 particles. Particles were extracted with box size of 400 pixels and the extraction was followed by several rounds of 2D classification that yielded 77,806 particles. Ab initio reconstruction on the clean particle stack with three classes and one round of heterogeneous refinement was conducted and resulted in the monomer and the dimer initial classes, where the dimer class had a significantly lower resolution than the

monomer one. Non-uniform refinement using a subset of particles for monomer and dimer resulted in a ~4 Å resolution density map corresponding to the monomer structure and an unsuccessful dimer reconstruction (Figure S2) (Punjani et al., 2020). Topaz particle picker was used to further enrich particles that belong to each oligomeric state (Bepler et al., 2019). Briefly, Topaz models were trained iteratively on small pools of particles, in which all particles were nearly unambiguously assigned to be either monomeric or dimeric. These pools were selected from the 25 micrographs with the highest number of particles identified with the template-based particle picking approaches. After each round of training, particles were extracted in 400-pixel boxes and 2D classification was used to filter out problematic particles. The cleaned particle stack was used for the next round of training. The training, particle extraction and 2D classification were conducted iteratively until the models for monomer and dimer stopped improving. The models were then used to pick particles from all micrographs. Note that each batch of data collected required separate Topaz training and extraction. Pooled monomer (779,882) and dimer (688,464) particles from two data collection batches were then processed separately via one round of 2D classification and 2–3 rounds of heterogeneous refinement to remove particles corresponding to contaminants. A set of 150,028 monomer particles entered the final non-uniform refinement and resulted in a 3.15 Å resolution map; a set of 40,700 dimer particles entered the final non-uniform refinement with C2 symmetry and resulted in a map of 3.46 Å resolution. No additional masking was applied beyond cryoSPARC's default dynamic masking procedure, and no sharpening was applied to the maps. The local resolution maps were generated using CryoSPARC Local Resolution Estimation job. An initial model was obtained by docking the PDB 6WTI to the map using MOLREP implemented in CCPEM (Vagin and Teplyakov, 1997; Burnley et al., 2017; Wood et al., 2015). Assignments of lipid densities to 1,2-distearoyl-sn-glycerophosphoethanolamine (3PE) were also based on PDB 6WTI. The model was then iteratively rebuilt manually in Coot and refined using *Phenix.real_space_refine* and Servalcat (Emsley and Cowtan, 2004; Krissinel and Henrick, 2004; Liebschner et al., 2019; Murshudov et al., 2011; Yamashita et al., 2021; Brown et al., 2015; Emsley et al., 2010; Afonine et al., 2018). UCSF Chimera was used for map visualization (Pettersen et al., 2004). Model summary statistics were generated by MolProbity (Chen et al., 2010) and Servalcat (Table 1). The atomic coordinates and maps have been deposited in the Protein Data Bank (http://wwpdb.org/) (PDB: 8F68 and 8F6C) and the Electron Microscopy Data Bank (https://www.ebi.ac.uk/emdb/) (EMD-28877 and EMD-28879).

TABLE 1 Data collection and processing.

	Data collection	
Instrument	Titan Krios G2	
Detector	K3 Summit	
Energy filter	No	
Objective aperture	No	
Nominal magnification	105,000×	
Data collection mode	Beam-Image Shift; 3 × 3 holes per movie	
Frames per movie	100	
Electron dose (e^{-}/A^{2}/frame)	0.8	
Exposure time (s/frame)	0.04	
Super-resolution mode	Yes	
Detector pixel size (Å)	0.834	
Data pixel size (Å)	0.417	
Movies acquired	6907 (batch 1: 2398; batch 2: 4509)	
	Reconstruction	
	Monomer	Dimer
Molecular weight (kDa)	143,929	284,020
Reconstruction symmetry	C1	C2
Total picked particles	779,882	688,464
Particles used in refinement	150,028	40,700
Resolution $FSC_{0.143}$ (Å)	3.15	3.46
	Refinement and validation	
	Monomer	Dimer
Non-hydrogen atoms	9741	19,494
Protein residues	1198	2396
Ligands	6	12
RMSD bond lengths (Å)	0.0042	0.0035
RMSD bond angles (°)	1.4056	1.3881
Model-to-map FSC (all)	0.73	0.66
MolProbity score	1.35	1.36
Clashscore (all atom)	6.33	4.99
Poor rotamers (%)	0	0.9
Ramachandran (%)		
Favored	98.07	97.52
Allowed	1.93	2.48
Outliers	0	0

3 | RESULTS

3.1 | Three-dimensional reconstruction of the ubiquinol oxidase monomer and dimer in the same sample

Initial 2D classification of particles picked from a single sample indicated the presence of both monomers and

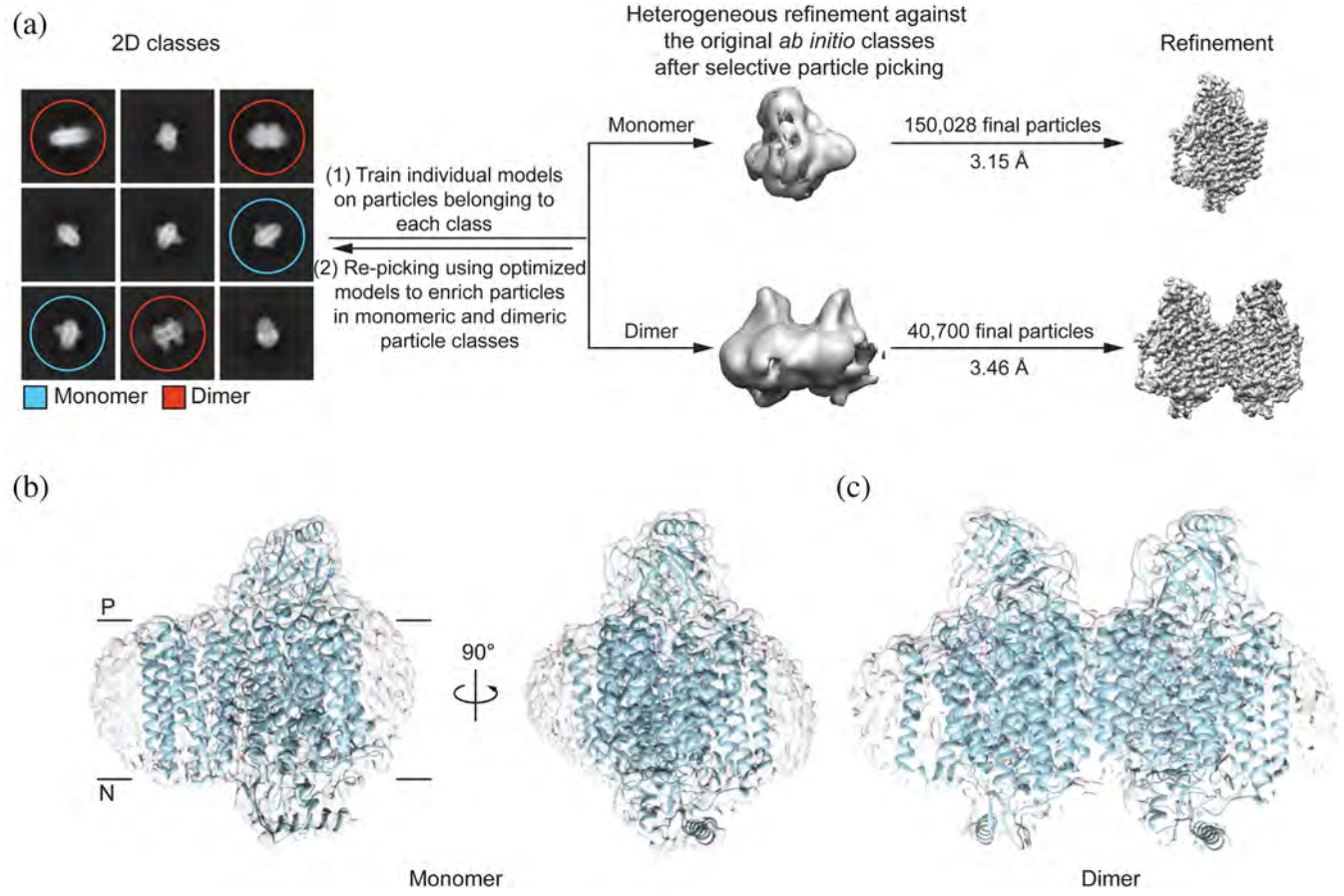

FIGURE 2 Cryo-EM reconstruction of the monomer and dimer structures of the *E. coli* ubiquinol oxidase. (a) General workflow for cryo-EM reconstruction. Left panel: selected 2D classes represent both monomers (cyan circles) and dimers (red circles). Note that monomer and dimer 2D projections from certain angles may look similar to each other. Such classes are not labeled with a colored circle. Middle panel: *heterogeneous reconstruction against* the two original ubiquinol oxidase classes (monomer and dimer). The dimer class has significantly lower abundance than the monomer class, so iterative AI-assisted particle picking was conducted to enrich the dimer class. Right panel: 3D maps of refined monomer (150,028 total particles, 3.15 Å resolution) and dimer (40,700 total particles, 3.46 Å resolution). (b) Map and atomic model of the ubiquinol oxidase monomer. (c) Map and atomic model of the ubiquinol oxidase dimer at contour level 0.05.

dimers of ubiquinol oxidases (Figures 2a and S2). However, particle picking using blob or template-based methods favors the monomer, likely due to the higher abundance of monomers in the sample (Figure S2). To enrich particles for each oligomeric status, we used Topaz, a CNN-based particle picker (Bepler et al., 2019). Several rounds of training and picking were performed, resulting in progressively purer sets of monomeric or dimeric particles at the end of each iteration, which were then used as the input for the next round of training. The final enriched sets of particles for each oligomeric state were then used in the next steps of the reconstruction process to obtain the final refined models. For the ubiquinol oxidase monomer, 150,028 particles were used in the final refinement and resulted in a 3.15 Å resolution map; for the dimer, 40,700 particles were used in the final refinement and the reconstructed map reached resolution of 3.46 Å (Figure S3a,b). The data collection and image processing are summarized in Table 1. In both the monomer and dimer maps, the transmembrane domain of the protein was surrounded by an amphipol ring, the position of which is consistent with lipid layer and/or nanodiscs positions in previously solved structures of this enzyme (PDB: 1FFT, 6WTI, 7CUW) (Figures 2b,c and S3c). The monomer to dimer ratio in the refinement subsets of particles is around 4:1, which is lower than the ratio observed in the BN-PAGE experiments described above (monomer: dimer = ~50:1) (Stenberg et al., 2007). Note that the reconstruction processes included a number of steps enriching for dimers. For this reason, the monomer to dimer ratio (4:1) observed in the analyzed subsets of particles may be non-physiological.

3.2 | Monomer structure of the ubiquinol oxidase

The structure of the ubiquinol oxidase monomer solved in this study is very similar to previously published results, with only differences in the number of bound ligands (Figures 2b and 3). All four subunits, including residues 552–656 in subunit I, which were missing in the first X-ray crystallographic structure (1FFT), showed clear density in the map of our reconstruction (EMD-28877) (Figure 2b) (Abramson et al., 2000). Our atomic model (8F68) is similar to the recently solved cryo-EM structures of this protein (7CUW and 6WTI) (Li et al., 2021; Su et al., 2021), with the Root Mean Square Deviation (RMSD) calculated between Cα atoms of our model and either of the two other models (7CUW and 6WTI) of ~0.4 Å (Figures 3a and S4a,b).

Both the heme *b* and the heme o_3 molecules are observed in the map at expected locations (Figure S4c). Specifically, the heme *b* molecule is coordinated by H106 and H421 from subunit I. Heme o_3 is coordinated by H419 of subunit I on one side, and the copper ion on the other. However, there is no density consistent with ubiquinone at the ubiquinone binding site (Figure 3b), which leaves the redox center of the protein incomplete. In addition, the map in this study showed three 1,2-distearoyl-sn-glycerophosphoethanolamine (3PE) molecules bound between subunit I and III, as observed in the published *E. coli* ubiquinol oxidase cryo-EM structures (Li et al., 2021; Su et al., 2021). Other ligands observed in the previously solved cryo-EM structures, such as additional 3PE molecules (observed in 7CUW subunit I and in 6WTI subunit I, II, and IV) and a pentadecyl(tetradecyl)peroxyanhydride (U9V) molecule (observed in 6WTI subunit I) were poorly resolved in our reconstruction, likely due to its lower resolution (3.15 Å), so they are not included in the atomic model. Lipids, such as 3PE, are frequently found associated with membrane proteins and are typically involved in protein folding and organization of protein supercomplexes (Krissinel and Henrick, 2005). Since the lipids we observe here are not considered part of the redox center and are not unique to the *E. coli* ubiquinol oxidase, they will not be further discussed.

3.3 | Dimer structure of the ubiquinol oxidase

The ubiquinol oxidase dimer (8F6C) has C2 symmetry, with the two-fold axis oriented parallel to the transmembrane domains (Figures 4a,c, and S5). Local resolution analysis of the map (EMD-28879) shows that most regions of the reconstruction have resolution close to the global resolution of the map (3.46 Å), with only the map region corresponding to TM0 of subunit I (Figure 4b, in red dashes circle) having significantly lower resolution (>4 Å), possibly due to higher flexibility arising from limited contacts between TM0 and the rest of the protein.

The dimerization interface is between subunit II of one monomer and subunit IV of the other monomer. The dimerization created a large channel between the two monomers, occupied by a few diffused densities likely arising from bound amphipol/lipids molecules (Figures 4c and S5a). The total buried interface area between the two monomers is ~556 A^2, which is ~0.6% of the total surface area of the dimer (87,166 A^2) (Krissinel and Henrick, 2005; Krissinel and Henrick, 2007). The dimerization interface is mostly nonpolar, and the hydrophobic interactions occur along the

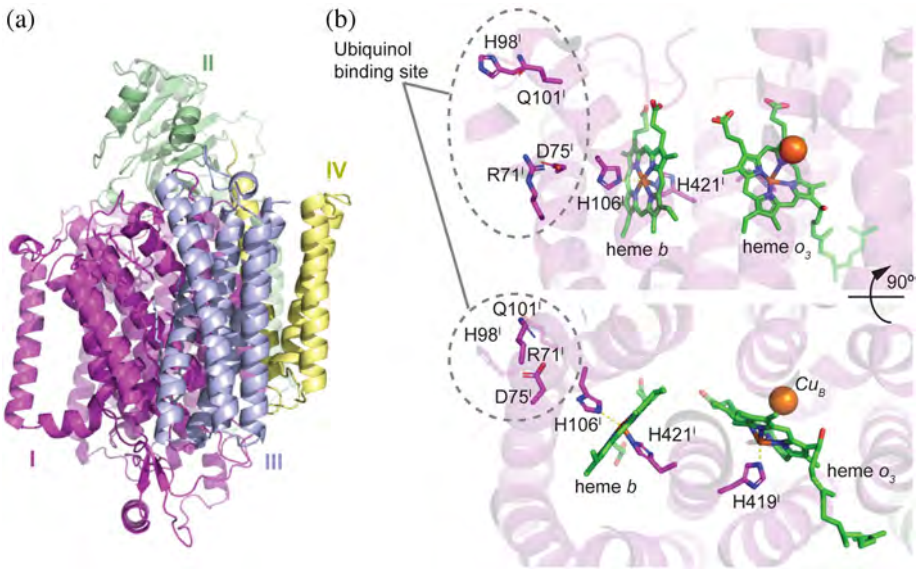

FIGURE 3 The *Escherichia coli* ubiquinol oxidase monomer structure. (a) Overview of the ubiquinol oxidase monomer structure solved in this study. The four subunits are labeled with color (I: magenta; II: green; III: blue; IV: yellow). (b) Detailed view of the redox center from two different angles (bottom panel is top panel rotated 90 degrees). The ubiquinol binding site is labeled with a gray dashed circle and key residues are shown ($R71^I$, $H98^I$, $Q101^I$). No ubiquinone molecule was observed in the structure. Heme *b* is coordinated with $H106^I$ and $H421^I$. Heme o_3 is coordinated with $H419^I$ and the copper ion is labeled as an orange sphere.

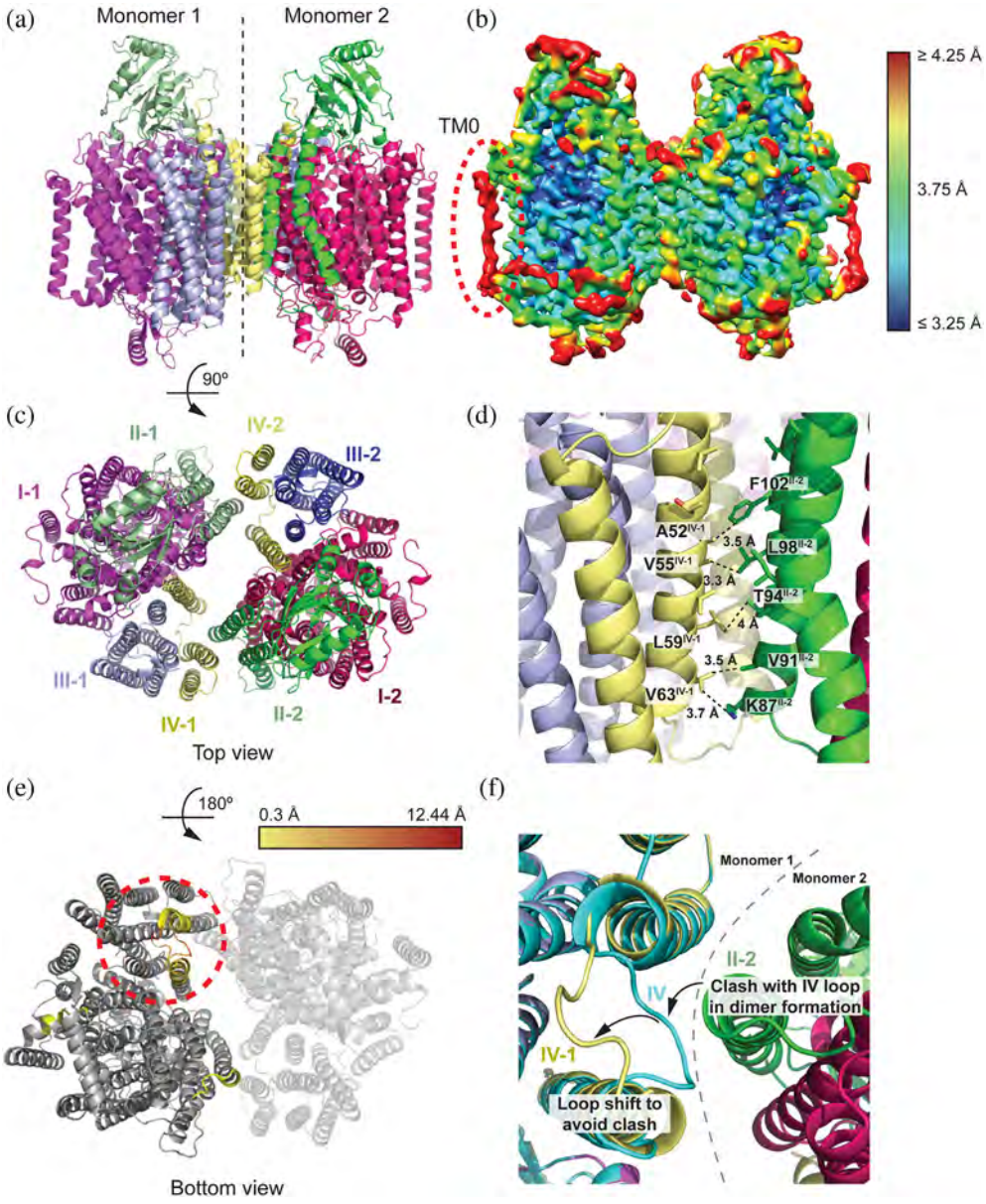

FIGURE 4 The *Escherichia coli* ubiquinol oxidase dimer structure. (a) Overview of the ubiquinol oxidase dimer structure solved in this study. The two monomers are separated by a dashed line in the middle. Color representation of the subunits is the same for monomer 1 as in Figure 3; brighter colors are used for monomer 2. (b) Local resolution of the dimer map. TM0 in subunit I shows the lowest resolution among all regions. (c) Top view of the dimer structure shown in panel a with each monomer and its subunits labeled in color. The dimer has C2 symmetry. (d) Key residues at the dimerization interface. In the dimer, subunit IV of monomer 1 interacts through a series of hydrophobic interactions with the subunit II of monomer 2. Key residues involved in the hydrophobic interaction and the interaction distances are labeled. (e) Bottom view of the dimer structure shown in panel a superimposed with the monomer structure determined in this study. Residues with superimposition RMSD lower than 0.3 Å are shown in gray, residues with superimposition RMSD higher than 0.3 Å are shown in a yellow-red gradient (Min RMSD: 0.01 Å, Max RMSD: 12.44 Å, Ave. RMSD: 0.12 Å). The red dashed circle indicates the region of the protein with the highest RMSD between the monomer and the monomeric subunit of the dimer. (f) Detailed view of the region with the highest RMSD between monomer and the monomeric subunit of the dimer. Subunit IV in the monomer structure is in cyan. Gray dashed line indicates the boundary between monomer 1 and monomer 2 in the dimer structure. Subunit IV of monomer 1 (IV-1) in the dimer structure is shown in yellow. Subunit II of monomer 2 (II-2) is shown in green. Arrows show the movement of the subunit IV loop position between the monomeric and dimeric structures. This movement is required to prevent clashes with subunit II of monomer 2 (II-2) upon dimer formation.

helices of subunit IV of monomer 1 (yellow) and subunit II of monomer 2 (green), where the two helices are almost parallel to each other (Figure 4d**)**. Key residues that participate in hydrophobic interactions between the two subunits are shown in Figure 4d. Specifically, V63 from subunit IV, monomer 1 interacts with side chains of

both K87 and V91 from subunit II, monomer 2. L59, V55, and A52 from subunit IV of monomer 1 form hydrophobic interactions with T97, L98 and F102 from subunit II of monomer 2 (Figure S5c). Beyond F102 of subunit II of monomer 2 (toward the C-terminus), the two parallel helices are too far from each other to engage in any interactions. Such large channel and small dimerization interface have been observed in bovine cytochrome *c* oxidase (C*c*O) dimer structure (Tsukihara et al., 1996). The channel in C*c*O was proposed to accommodate lipids to stabilize dimerization ("lipid shield") and that hypothesis was supported by mass spectrometry data and by weak lipid densities observed in a 1.3 Å resolution structure (Liko et al., 2016; Shinzawa-Itoh et al., 2021). Although C*c*O structure is not close enough to the *E. coli* ubiquinol oxidase to enable direct structural comparison, we believe that the channel of the *E. coli* ubiquinol oxidase could play a similar role and harbor lipid molecules. However, due to limited resolution of our reconstruction, we cannot model structurally the observed diffused densities.

The monomeric subunit in the ubiquinol oxidase dimer structure (8F6C) is very similar to the ubiquinol oxidase monomer structure (8F68), with the RMSD of 0.624 Å based on the alignment of Cα atoms from 1204 residues (alignment on one monomer). Figures 4e and S5b shows the superimposition of the monomer and the dimer structures; regions with superimposed RMSD higher than 0.3 Å are highlighted in a gradient of yellow and red. The most significant difference is located in the loop in subunit IV (residues 67–74) (Figure 4e, red dashed circle, Figure 4f). Before the dimer formation, this loop is positioned outward towards the surface of the protein (Figure 4f, cyan). After the dimer formation, subunit II of monomer 2 forces the loop to move away from the dimer interface to avoid a clash (Figure 4f, yellow). The maximum shift of the loop position is ~12 Å between the monomer and dimer states. The loop region has relatively low local resolution in both the monomer and the dimer maps, which suggests that this region is dynamic (Figure S5d).

4 | DISCUSSION AND CONCLUSION

In this study, we report two *E. coli* cytochrome bo_3 ubiquinol oxidase structures. The monomer structure was reconstructed at 3.15 Å, a lower resolution than the published cryo-EM structures 7CUW (resolution 2.63 Å) and 6WTI (resolution 2.38 Å) (Li et al., 2021; Su et al., 2021). The dimer structure was reconstructed at an intermediate resolution of 3.46 Å and is the first dimer structure reported for this protein.

A few points are worth mentioning about the structures solved in this study in comparison to the published structures (Abramson et al., 2000; Li et al., 2021; Su et al., 2021). Firstly, amphipol was used in this study to maintain the solubility of the membrane protein, instead of detergent, styrene maleic acid co-polymer (SMA) or nanodiscs. The use of amphipol does not seem to affect the overall structure of the monomer, as the RMSD of the superposition between our structure and the previously reported structures is low. Secondly, both the monomer and the dimer structures lack the ubiquinone molecule bound to subunit I, which results in the incomplete redox center. It has been reported that certain detergents such as Triton X-100 could strip the bound ubiquinone from the protein (Puustinen et al., 1996). Only DDM and amphipol, which are routinely used in purification of similar ubiquinone-bound enzymes were used during purification in our study, so it is unclear at which step ubiquinone was lost from the protein (Li et al., 2021; Thesseling et al., 2019). Although the ubiquinone was missing in the structures, the lack of this cofactor is unlikely to be the reason for the dimerization, because: (1) the ubiquinone binding site is relatively distant from the dimerization interface; and (2) the ubiquinone is missing in the monomeric X-ray structure of this enzyme (1FFT) (Abramson et al., 2000). DDM was also used in the study by Stenberg, et al. where the ubiquinol oxidase dimer was observed on BN-PAGE, suggesting that DDM may preserve the dimer better than other detergents (e.g., Triton X-100) (Musatov et al., 1999; Stenberg et al., 2007). Thirdly, the measured dimerization interface is relatively small and covers only a small portion of the entire protein surface. However, this does not necessarily mean that the dimer structure is an experimental artifact since such small dimerization interfaces have been observed in both functionally related (bovine cytochrome *c* oxidase) and unrelated (O-linked beta-*N*-acetylglucosamine transferase) proteins (Tsukihara et al., 1996; Meek et al., 2021). Further experiments are required to determine whether the dimer is functional and/or physiologically relevant.

To summarize, in this study we solved the structures of the *E. coli* ubiquinol oxidase in two oligomeric states (monomer and dimer) from the same sample. The monomer structure, despite its intermediate resolution and the lack of ubiquinone cofactor, is highly consistent with the other published results and adds support to previously observed orientation for residues 552–656 in subunit I that was missing in the X-ray crystallographic structure (1FFT) (Abramson et al., 2000). The dimer structure shows that the protein dimerizes in C2 symmetry through mainly hydrophobic interactions between subunit II from one monomer and subunit IV from the other monomer, with minor structural changes in the other

parts of the protein. Since it is the first dimer structure solved for the *E. coli* ubiquinol oxidase, it provides the groundwork for future hypothesis testing (e.g., sites for mutagenesis) regarding the physiologically relevant oligomeric state and functions of this protein.

AUTHOR CONTRIBUTIONS

Yirui Guo: Conceptualization (lead); data curation (lead); formal analysis (lead); funding acquisition (lead); investigation (lead); methodology (lead); project administration (supporting); validation (lead); visualization (lead); writing – original draft (lead); writing – review and editing (lead). **Elina Karimullina:** Conceptualization (supporting); data curation (supporting); formal analysis (supporting); investigation (lead); methodology (lead); validation (lead); visualization (supporting); writing – original draft (supporting); writing – review and editing (supporting). **Tabitha Emde:** Investigation (supporting). **Zbyszek Otwinowski:** Conceptualization (supporting); data curation (supporting); formal analysis (supporting); funding acquisition (lead); methodology (supporting); resources (lead). **Alexei Savchenko:** Conceptualization (supporting); formal analysis (supporting); funding acquisition (lead); investigation (supporting); methodology (supporting); project administration (lead); resources (lead); supervision (lead); writing – original draft (supporting); writing – review and editing (supporting).

ACKNOWLEDGMENTS

This project has been funded in whole or in part with federal funds from the National Institute of Allergy and Infectious Diseases, National Institutes of Health, Department of Health and Human Services, under Contracts HHSN272201700060C and 75N93022C00035. This project was also supported by funds from the Department of Energy (DE-SC0019600 to YG and ZO, DE-SC0021600 to ZO) and funds from the National Institute of General Medical Sciences, National Institutes of Health (R35GM145365 to ZO).

We thank the Cryo-Electron Microscopy Facility (CEMF) at UT Southwestern Medical Center which has been supported by grants RP170644 and RP220582 from the Cancer Prevention and Research Institute of Texas (CPRIT) for maintaining a Titan Krios microscope.

CONFLICT OF INTEREST STATEMENT

Yirui Guo, Zbyszek Otwinowski, and Dominika Borek are co-founders of Ligo Analytics. Yirui Guo serves as the CEO of Ligo Analytics.

DATA AVAILABILITY STATEMENT

The atomic coordinates (8F68; PDB DOI: 10.2210/pdb8F68/pdb and 8F6C; PDB DOI: 10.2210/pdb8F6C/pdb) and maps (EMD-28877 and EMD-28879)have been deposited in the Protein Data Bank (http://wwpdb.org/) and the Electron Microscopy DataBank (https://www.ebi.ac.uk/emdb/), respectively.

ORCID

Dominika Borek https://orcid.org/0000-0002-4321-6253
Alexei Savchenko https://orcid.org/0000-0002-5256-9237

REFERENCES

Abramson J, Riistama S, Larsson G, Jasaitis A, Svensson-Ek M, Laakkonen L, et al. The structure of the ubiquinol oxidase from Escherichia coli and its ubiquinone binding site. Nat Struct Biol. 2000;7:910–7.

Afonine PV, Poon BK, Read RJ, Sobolev OV, Terwilliger TC, Urzhumtsev A, et al. Real-space refinement in PHENIX for cryo-EM and crystallography. Acta Crystallogr D Struct Biol. 2018;74:531–44.

Bepler T, Morin A, Rapp M, Brasch J, Shapiro L, Noble AJ, et al. Positive-unlabeled convolutional neural networks for particle picking in cryo-electron micrographs. Nat Methods. 2019;16:1153–60.

Brown A, Long F, Nicholls RA, Toots J, Emsley P, Murshudov G. Tools for macromolecular model building and refinement into electron cryo-microscopy reconstructions. Acta Crystallogr D Biol Crystallogr. 2015;71:136–53.

Burnley T, Palmer CM, Winn M. Recent developments in the CCP-EM software suite. Acta Crystallogr D Struct Biol. 2017;73:469–77.

Chen VB, Arendall WB, Headd JJ, Keedy DA, Immormino RM, Kapral GJ, et al. MolProbity: all-atom structure validation for macromolecular crystallography. Acta Crystallogr D. 2010;66:12–21.

Emsley P, Cowtan K. Coot: model-building tools for molecular graphics. Acta Crystallogr D Biol Crystallogr. 2004;60:2126–32.

Emsley P, Lohkamp B, Scott WG, Cowtan K. Features and development of coot. Acta Crystallogr D Biol Crystallogr. 2010;66:486–501.

Krissinel E, Henrick K. Secondary-structure matching (SSM), a new tool for fast protein structure alignment in three dimensions. Acta Crystallogr D Biol Crystallogr. 2004;60:2256–68.

Krissinel E, Henrick K. Detection of protein assemblies in crystals. Lect Notes Comput Sc. 2005;3695:163–74.

Krissinel E, Henrick K. Inference of macromolecular assemblies from crystalline state. J Mol Biol. 2007;372:774–97.

Li J, Han L, Vallese F, Ding Z, Choi SK, Hong S, et al. Cryo-EM structures of Escherichia coli cytochrome Bo 3 reveal bound phospholipids and ubiquinone-8 in a dynamic substrate binding site. Proc Natl Acad Sci U S A. 2021;118(34):e2106750118.

Liebschner D, Afonine PV, Baker ML, Bunkoczi G, Chen VB, Croll TI, et al. Macromolecular structure determination using X-rays, neutrons and electrons: recent developments in Phenix. Acta Crystallogr D Struct Biol. 2019;75:861–77.

Liko I, Degiacomi MT, Mohammed S, Yoshikawa S, Schmidt C, Robinson CV. Dimer interface of bovine cytochrome c oxidase is influenced by local posttranslational modifications and lipid binding. Proc Natl Acad Sci U S A. 2016;113:8230–5.

Mastronarde DN. Automated electron microscope tomography using robust prediction of specimen movements. J Struct Biol. 2005;152:36–51.

Meek RW, Blaza JN, Busmann JA, Alteen MG, Vocadlo DJ, Davies GJ. Cryo-EM structure provides insights into the dimer arrangement of the O-linked beta-N-acetylglucosamine transferase OGT. Nat Commun. 2021;12:6508.

Murshudov GN, Skubak P, Lebedev AA, Pannu NS, Steiner RA, Nicholls RA, et al. REFMAC5 for the refinement of macromolecular crystal structures. Acta Crystallogr D Biol Crystallogr. 2011;67:355–67.

Musatov A, Ortega-Lopez J, Demeler B, Osborne JP, Gennis RB, Robinson NC. Detergent-solubilized Escherichia coli cytochrome bo3 ubiquinol oxidase: a monomeric, not a dimeric complex. FEBS Lett. 1999;457:153–6.

Pettersen EF, Goddard TD, Huang CC, Couch GS, Greenblatt DM, Meng EC, et al. UCSF chimera—a visualization system for exploratory research and analysis. J Comput Chem. 2004;25:1605–12.

Punjani A, Rubinstein JL, Fleet DJ, Brubaker MA. cryoSPARC: algorithms for rapid unsupervised cryo-EM structure determination. Nat Methods. 2017;14:290–6.

Punjani A, Zhang HW, Fleet DJ. Non-uniform refinement: adaptive regularization improves single-particle cryo-EM reconstruction. Nat Methods. 2020;17:1214–21.

Puustinen A, Finel M, Virkki M, Wikstrom M. Cytochrome o (bo) is a proton pump in Paracoccus denitrificans and Escherichia coli. FEBS Lett. 1989;249:163–7.

Puustinen A, Verkhovsky MI, Morgan JE, Belevich NP, Wikstrom M. Reaction of the Escherichia coli quinol oxidase cytochrome bo3 with dioxygen: the role of a bound ubiquinone molecule. Proc Natl Acad Sci U S A. 1996;93:1545–8.

Robinson NC, Talbert L. Triton X-100 induced dissociation of beef heart cytochrome c oxidase into monomers. Biochemistry. 1986;25:2328–35.

Shinzawa-Itoh K, Hatanaka M, Fujita K, Yano N, Ogasawara Y, Iwata J, et al. The 1.3-Å resolution structure of bovine cytochrome c oxidase suggests a dimerization mechanism. BBA Advances. 2021;1:100009.

Si D, Nakamura A, Tang RB, Guan HW, Hou J, Firozi A, et al. Artificial intelligence advances for de novo molecular structure modeling in cryo-electron microscopy. Wires Comput Mol Sci. 2022;12:e1542.

Skalidis I, Kyrilis FL, Tuting C, Hamdi F, Chojnowski G, Kastritis PL. Cryo-EM and artificial intelligence visualize endogenous protein community members. Structure. 2022;30:575–589.e6.

Sone N, Kosako T. Evidence for dimer structure of proton-pumping cytochrome c oxidase, an analysis by radiation inactivation. EMBO J. 1986;5:1515–9.

Stenberg F, von Heijne G, Daley DO. Assembly of the cytochrome bo3 complex. J Mol Biol. 2007;371:765–73.

Su CC, Lyu M, Morgan CE, Bolla JR, Robinson CV, Yu EW. A 'Build and Retrieve' methodology to simultaneously solve cryo-EM structures of membrane proteins. Nat Methods. 2021;18:69–75.

Thesseling A, Rasmussen T, Burschel S, Wohlwend D, Kagi J, Muller R, et al. Homologous bd oxidases share the same architecture but differ in mechanism. Nat Commun. 2019;10:5138.

Tsukihara T, Aoyama H, Yamashita E, Tomizaki T, Yamaguchi H, Shinzawa-Itoh K, et al. The whole structure of the 13-subunit oxidized cytochrome c oxidase at 2.8 A. Science. 1996;272:1136–44.

Vagin A, Teplyakov A. MOLREP: an automated program for molecular replacement. J Appl Cryst. 1997;30:1022–5.

Wood C, Burnley T, Patwardhan A, Scheres S, Topf M, Roseman A, et al. Collaborative computational project for electron cryo-microscopy. Acta Crystallogr D Biol Crystallogr. 2015;71:123–6.

Yamashita K, Palmer CM, Burnley T, Murshudov GN. Cryo-EM single-particle structure refinement and map calculation using Servalcat. Acta Crystallogr D Struct Biol. 2021;77:1282–91.

Yu CA, Xia D, Kim H, Deisenhofer J, Zhang L, Kachurin AM, et al. Structural basis of functions of the mitochondrial cytochrome bc1 complex. Biochim Biophys Acta. 1998;1365:151–8.

Zhang Z, Huang L, Shulmeister VM, Chi YI, Kim KK, Hung LW, et al. Electron transfer by domain movement in cytochrome bc1. Nature. 1998;392:677–84.

SUPPORTING INFORMATION

Additional supporting information can be found online in the Supporting Information section at the end of this article.

How to cite this article: Guo Y, Karimullina E, Emde T, Otwinowski Z, Borek D, Savchenko A. Monomer and dimer structures of cytochrome bo_3 ubiquinol oxidase from *Escherichia coli*. Protein Science. 2023;32(4):e4616. https://doi.org/10.1002/pro.4616